Proton density and orientational potential in nickelhexammine salts: a thermodynamic analysis of rotation-translation coupling

1994 J. Phys.: Condens. Matter 6 10989

(http://iopscience.iop.org/0953-8984/6/50/009)

J. Phys.: Condens. Matter 6 (1994) 10989–11005. Printed in the UK

Proton density and orientational potential in nickelhexammine salts: a thermodynamic analysis of rotation–translation coupling

P Schiebel†, A Hoser†§, W Prandl†, G Heger‡‖, W Paulus‡ and P Schweiss‡¶

† Institut für Kristallographie, Universität Tübingen, D-72070 Tübingen, Germany

‡ Laboratoire Léon Brillouin, CEA-CNRS Saclay, F-91191 Gif-sur-Yvette, France

Received 4 July 1994

Abstract. The scattering densities of the orientationally disordered protons and deuterons in $Ni(NX_3)_6Y_2$ (X = H or D; Y = Br, I, NO_3 or PF_6) are obtained from neutron single-crystal diffraction data at room temperature. While we observe a nearly circular density distribution for Y = PF_6, a nuclear density distribution with four maxima on a square shows up for Y = Br, I and NO_3. This is a pronounced deviation from the circular distribution that is expected from uniaxial rotational diffusion or reorientational jump models for the dynamics of the orientational disordered ammonia groups. All observed density distributions are consistently explained as the consequence of rotation–translation coupling in an anharmonic crystal potential. The calculated potential parameters, i.e. anharmonicity and strength of the coupling, depend on the type of anion present in the crystal frame. The weak anisotropy in the Y=NO_3 and PF_6 compounds is the consequence of a nearly eightfold non-crystallographic symmetry of the atoms establishing the hindrance potential.

1. Introduction

Metalhexammine complexes with the chemical composition $M(NX_3)_6Y_2$, where M is a transition-metal ion, Y an ordinary or complex anion of valence one, and X = H or D, have been thoroughly investigated during the last three decades mostly for two reasons. The first is because they have a sequence of phase transitions that all derive from a cubic parent phase with the space group $Fm3m$. The second reason, coupled to the first, is the orientational disorder of the NH_3/ND_3 groups observed in the high- as well as low-temperature phases. The reason for this disorder, at least in the cubic parent phase, is the incompatibility of the molecular symmetry ($3m$) with the site symmetry ($4mm$) in the crystal. Phase transitions in this family of compounds (with M = Ni) were reported for the first time in 1960 [1]. The transition temperatures T_c found depend on the anions Y as well as on the cations M [2, 3]. In addition, an isotropic effect of T_c is clearly visible when the protons are replaced by deuterons [4–6]. The molecular orientational disorder has been investigated by quasielastic as well as by high-resolution inelastic neutron scattering (QNS/INS). A short review and comparison of QNS, Raman and specific-heat data for some Ni and Mg compounds has

§ Present address: Institut für Physikalische Chemie und Elektrochemie der Universität Hannover, D-30167 Hannover, Germany.

‖ Present address: Institut für Kristallographie, RWTH Aachen, D-52062 Aachen, Germany.

¶ On leave from Kernforschungszentrum Karlsruhe, INFP, D-76021 Karlsruhe, Germany.

0953-8984/94/5010989+17$19.50

been given recently [7]. At low temperatures, tunnel splitting due to NH_3 motions has been found [7–9].

Bates and Stevens gave a first theoretical picture of the phase transition in 1969 [10], which was later extended by Bates *et al* [11]. Following Bates and Stevens the essential interaction is the interaction between neighbouring $Ni(NH_3)_6$ clusters, whereas interactions with the anions are neglected. Using a point-charge model these authors find eight minimum energy configurations for the NH_3 groups, among which the six NH_3 groups of a $Ni(NH_3)_6$ cluster are assumed to move independently in the high-temperature phase in such a way that an averaged octahedral crystal field is generated at the Ni site by fast reorientations. On cooling, the jump rates are predicted to diminish and trigonal distortion is preferred. In 1970 Elgsaeter and Svare suggested [12] an additional displacive component by taking into account the cluster–anion interaction: as a result, distortions of lower symmetry than suggested by the Bates–Stevens model were predicted. Eckert and Press [5] found indeed a weak trigonal distortion in $Ni(NH_3)_6I_2$, whereas $Ni(NH_3)_6Cl_2$ [13] and $Fe(NH_3)_6Cl_2$ [2] as well as compounds with complex anions [4, 14] distort more strongly in a monoclinic way. $Ni(NH_3)_6(PF_6)_2$ is exceptional in the Ni family of compounds in that it stays cubic down to 4 K.

Two competing models have been applied to interpret the QNS data: a model using 120° jumps of the NH_3 groups [4] and a uniaxial rotational diffusion model [4, 5]. Janik *et al* [7] have compared both models, using QNS data of the $Ni(NH_3)_6Br_2$ [15], $Ni(NH_3)_6Cl_2$ [16] and $Ni(NH_3)_6(BF_4)_2$ [17] compounds: they find no essential differences. A discrete 120° jump model of molecular reorientations would clearly favour the discrete Bates–Stevens model of the high-temperature parent phase, whereas a rotational diffusion model would agree better with a continuous density distribution. It is with this question in mind that we started a crystallographic investigation of the family of Ni compounds.

We found in an investigation of the disorder and the rotational potential of the NO_3 group in $Ni(NH_3)_6(NO_3)_2$, more or less as a by-product, that the protons were distributed over the corners of a square [18]. In later contributions we developed a thermodynamic model that explains this phenomenon as the coupling of rotation and translation in a highly anharmonic crystal potential for the $Ni(NH_3)_6Br_2$ [19, 20] and the $Ni(NH_3)_6I_2$ compounds [21].

In the present paper we use our earlier $Ni(NH_3)_6(NO_3)_2$ data [18] and new data for $Ni(NH_3)_6Br_2$ as well as for $Ni(NH_3)_6(PF_6)_2$ to give a more complete set of crystal potentials V_{Cr}, their correlations with the effective anion size, and some molecular-dynamics simulations of the proton/deuteron orbits.

The paper is organized as follows: a minimum of experimental details is given in section 2. In section 3 we review briefly the basic features of the crystal structure and of the techniques used to prepare the disordered hydrogen/deuteron densities from the experimental data. Section 4 deals with the *ansatz* for the two-dimensional crystal potential, which is the basis of the rotation–translation coupling, and with the crystal potentials derived.

In section 5 we introduce the effective potential, which is the sum of the crystal potential probed by the three protons/deuterons. In the concluding section 6 the limitations of the *ansatz* chosen (Boltzmann versus quantum statistics), the correlations between ionic radii and potential parameters, and the consequences of the present paper for the observation of free rotation of molecules in crystals are given.

2. Experimental details

Single crystals were synthesized from aqueous solutions by standard techniques [22].

Samples are prepared by dissolving $Ni(OH)_2 \cdot 6H_2O$ in concentrated ammonia solution to give $Ni(NH_3)_6(OH)_2$. Adding NH_4Y (Y=Br, I, NO_3, PF_6) and heating to 70 °C yields an oversaturated solution. By slowly cooling down (1 °C/day) to room temperature, single crystals with blue colour and octahedral shape grow. Deuterated single crystals are grown by using the appropriate deuterated materials.

Neutron diffraction data at room temperature were collected on the four-circle diffractometer C2 at the hot source of the ORPHÉE reactor in Saclay, with the exception of the $Ni(NH_3)_6(NO_3)_2$, which was measured at SILOE/CENG, Grenoble [18].

3. Scattering density

3.1. Crystal structure

At room temperature nickel hexammine compounds $Ni(NX_3)_6Y_2$ form face centred cubic crystals (space group $Fm3m$), with the hexammine clusters at the corners and the face centres of a cube and the anions Y at the $(\pm\frac{1}{4}, \pm\frac{1}{4}, \pm\frac{1}{4})$ positions (figure 1). Thus the crystal structure is essentially a decorated fluorite structure. The basic unit is a cube of Y ions that surround one $Ni(NX_3)_6$ octahedron. The lattice parameter a ranges from 10.382 to 11.933 Å among the studied compounds depending on the anion (table 1). Each nickel hexammine cluster consists of a central nickel ion surrounded octahedrally by six ammonia groups. The nitrogen atoms are located at the fourfold axes at $(\pm x, 0, 0)$, $(0, \pm x, 0)$, $(0, 0, \pm x)$ plus face centring. The proton/deuteron triangles point away from the central metal ion. Frustration arises from the molecular threefold symmetry ($3m$) of the NH_3/ND_3 group and the fourfold symmetry ($4mm$) of its site in the cubic unit cell. This results in the dynamic disorder of the ammine group and hence in its delocalization.

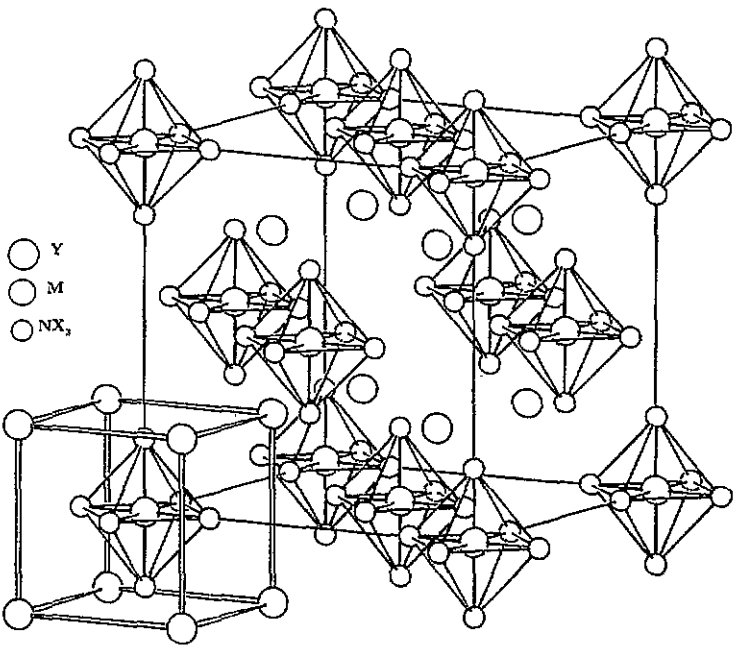

Figure 1. Schematic view of the crystal structure.

Table 1. Distances derived from the structural refinement.

	a (Å)	r_Y^{ion} (Å)	z_N (Å)	h_{NH_3} (Å)	r_p^1 (Å)	r_p^{XX} (Å)	r_p^{0Y} (Å)
$Ni(ND_3)_6Br_2$	10.382	1.96	2.136(2)	0.359(2)	0.921(4)	0.76(1)	1.04(1)
$Ni(NH_3)_6Br_2$	10.382	1.96	2.136(2)	0.369(5)	0.950(9)	0.64(3)	1.09(2)
$Ni(NH_3)_6I_2$	10.875	2.20	2.135(2)	0.380(2)	0.939(5)	0.88(2)	1.09(2)
$Ni(NH_3)_6(NO_3)_2$	10.881		2.111(2)	0.384(6)	0.949(5)	0.943(7)	0.948(8)
$Ni(NH_3)_6(PF_6)_2$	11.933		2.144(4)	0.402(7)	0.934(8)	0.91(3)	0.96(2)

We reported earlier our structure analysis for $Ni(NH_3)_6(NO_3)_2$, $Ni(ND_3)_6Br_2$ and $Ni(NH_3)_6I_2$ [18, 19, 21] where the density of the NH_3/ND_3 groups was treated by density interpolation. The structure refinement was carried out with SHELX [23]. The same analysis was used for $Ni(NH_3)_6Br_2$ and $Ni(NH_3)_6(PF_6)_2$ [24]. The basic idea behind density interpolation is to replace a disordered atom or molecule by a fictitious larger number of fractional atoms (split-atom model) or fractional groups (Frenkel or split-molecule model) undergoing harmonic motion. The weighted sum of these fractional atoms or groups is chosen equal to the actual number existing in the unit cell. All positions and thermal motion parameters are then fitted to the data as closely as possible.

All models for the studied compounds reveal that the H_3/D_3 density is concentrated in a plane that is perpendicular to the respective Ni–N axis. From the structure refinement we determined the distance z_N between the nickel and the nitrogen ion, and the distance h_{NH_3} between the nitrogen ion and the intersection of the fourfold crystal axis with the proton plane (table 1). Both values turn out to be independent of the model used for the distribution of the hydrogen atoms. In contrast we obtain three different values for the rotation radius r_p, i.e. the distance from the protons to the fourfold axis, depending on the specific type of model: r_p^1 is obtained from a split-atom model where eight symmetry-equivalent fractional protons/deuterons (weight 3/8) are refined; r_p^{0Y} and r_p^{XX} result from Frenkel models for which the molecular mirror plane coincides with one of the crystal mirror planes, thus leading to 12 hydrogen positions.

If no tumbling is present h_{NH_3} and r_p should correspond to the height of an ammonia pyramid, h, and the rotational radius, d_p, i.e. the distance from the protons to the threefold molecular axis, respectively (NH_3 gas: $h = 0.370$ Å, $d_p = 0.937$ Å; ND_3 gas: $h = 0.381$ Å, $d_p = 0.940$ Å [25]). Beyond that, if the ammonia molecules undergo uniaxial rotational diffusion, which means equal probability of occupying any position on a ring, the resulting radius should be independent of the underlying model and $d_p = r_p^1 = r_p^{0Y} = r_p^{XX}$ should be valid. If, however, the ammonia molecules show jump diffusion, we would expect a circular density distribution with a 12-fold modulation. This should be best described by one of the two models with 12 hydrogen positions on a ring.

What we find is that h_{NH_3} corresponds very well to the height of an undistorted ammonia pyramid. Together with the above-mentioned observation that the proton/deuteron density is concentrated on a plane perpendicular to the fourfold axis, a large tumbling motion of the ammonia is ruled out. On the other hand r_p clearly depends on the model used; moreover, only r_p^1 from the phenomenological split-atom model reflects the rotation radius of the ammonia molecule, but it does not give any direct insight into the underlying molecular dynamics.

3.2. Proton/deuteron densities

The importance of parametric models (Frenkel and split-atom models) follows from the stability of the phases of the calculated structure factors, i.e. their independence with respect

to the parameters refined from different models. It is this uniqueness of the calculated phases which makes density interpolation a reliable tool in the analysis of disordered density distributions. From the measured structure factors together with these stable phases it is possible to reconstruct a 'model-free' scattering density by Fourier synthesis [21, 24].

In our further analysis we are only interested in the disordered hydrogen density. Therefore we calculate the Fourier density of the ordered part of the structure, which is very well described by conventional structure analysis (SHELX [23]) and subtract it from the Fourier density derived from the measured $F_{obs}(H) \sim [I(H)]^{1/2}$ and the reconstructed phases. A detailed description of the method is given in [21, 24]. Figure 2 shows sections through the hydrogen density distributions obtained. A nearly circular density distribution is found only in $Ni(NH_3)_6(PF_6)_2$. Obviously the observed proton/deuteron distributions in $Ni(ND_3)_6Br_2$, $Ni(NH_3)_6Br_2$, $Ni(NH_3)_6I_2$ and $Ni(NH_3)_6(NO_3)_2$ are not circular. Instead of this we find four maxima on the corners of a square. The distances between these maxima are not compatible with distances in an ammonia molecule. The distribution of three H/D atoms over four corners of a square reveals a strange departure from the distribution that would be generated by an orientationally disordered ammonia molecule without rotation–translation coupling. As discussed above, this would lead to a distribution on a circle with modulations $\sim \cos(12n\varphi)$.

4. Rotation–translation coupling

4.1. Potential ansatz

From the results of the structure analysis discussed in section 3.1, the quasi-two-dimensional nature of the proton or deuteron density becomes evident. Thus the observed proton density is assumed to be generated by three protons that form a rigid and equilateral triangle. This proton triangle undergoes an anharmonic movement in a plane perpendicular to the fourfold axis at $z = z_H$, where the maximum of the proton density is found. One single setting of the triangle is then described by (R_c, ϕ_c), the radial coordinates of its centre of mass (CM), and the rotation angle β for rotation of the whole group around its CM (figure 3). The triangle moves in a crystal potential V_{Cr}, which must have the symmetry of the two-dimensional point group $4mm$ corresponding to the site symmetry $4mm$ on the fourfold axis

$$V_{Cr}(x, y) = V_{Cr}(r, \phi) = \tfrac{1}{2}Ar^2 + \tfrac{1}{4}Br^4\cos(4\phi) + \tfrac{1}{4}Cr^4. \tag{1}$$

This *ansatz* is exact up to terms $\sim r^4$. We have, tentatively, included a term $\sim r^6$ in our refinements, however, without essential improvements. From a purely formal point of view the term $\frac{1}{2}Ar^2$ seems to be a harmonic contribution. In reality all the 'A's we determine (see table 2) are negative. Indeed (1) is, with $B = 0$, the rotationally symmetry 2D generalization of the well known (2, 4) double-well potential, and $B \neq 0$ introduces the tetragonal symmetry. $|B| + C$ is a measure for the anharmonicity of the potential, while B denotes the strength of the anisotropy. The confinement of the molecules is guaranteed with $C > |B|$. Additionally, $A < 0$, $C > |B|$ leads to four potential minima at

$$r_m = \left(\frac{|A|}{C - |B|}\right)^{1/2} \qquad \phi_m = \pm 45°, \pm 135°$$

and four saddle points at

$$r_s = \left(\frac{|A|}{C + |B|}\right)^{1/2} \qquad \phi_m = 0°, \pm 90°, 180°.$$

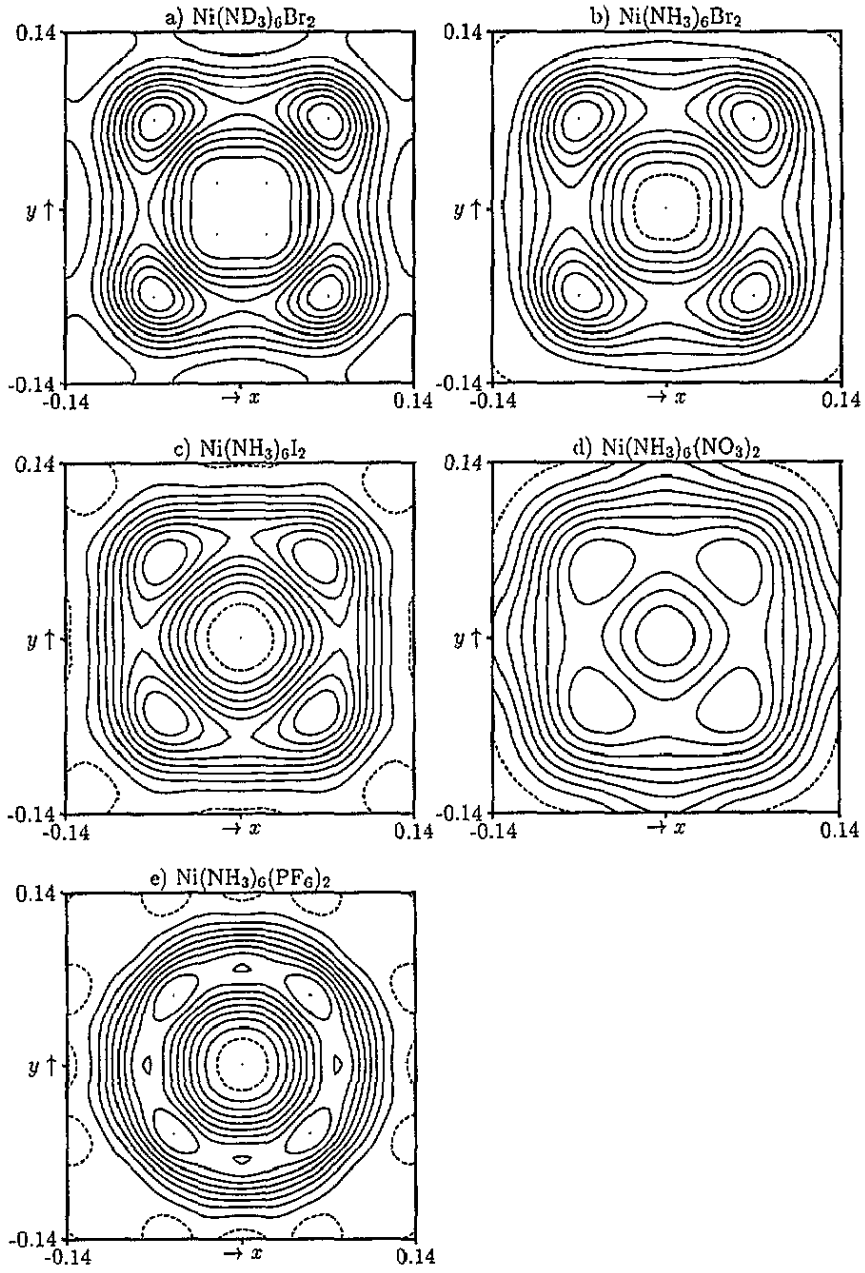

Figure 2. Observed proton/deuteron number densities, 10 level lines (dashed < 0) between ρ_{min} and ρ_{max}: (*a*) $Ni(ND_3)_6Br_2$, $z_D = 0.243a$; (*b*) $Ni(NH_3)_6Br_2$, $z_H = 0.241a$; (*c*) $Ni(NH_3)_6I_2$, $z_H = 0.231a$; (*d*) $Ni(NH_3)_6(NO_3)_2$, $z_H = 0.230a$; (*e*) $Ni(NH_3)_6(PF_6)_2$, $z_H = 0.213a$.

With $B = 0$ the potential becomes rotationally symmetric and instead of four minima a rotational miminum valley with

$$r_v = r_m = r_b = (|A|/C)^{1/2}$$

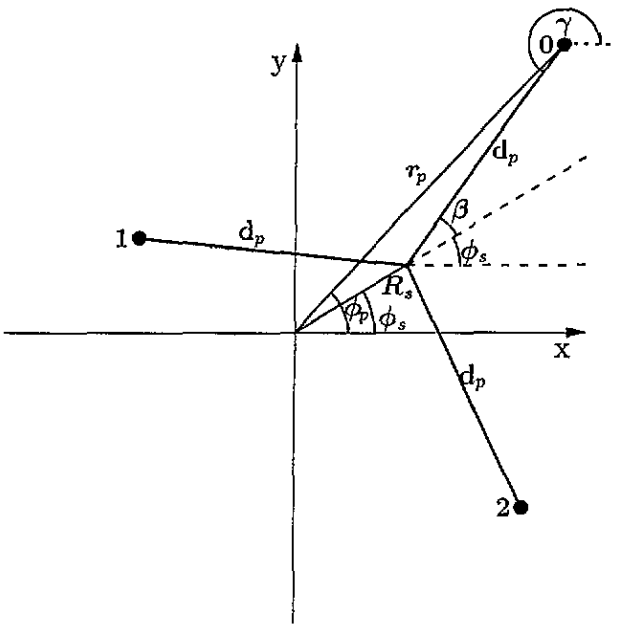

Figure 3. Geometric quantities defining the model.

exists. Therefore $\Delta r = r_m - r_s$ measures the anisotropy of the potential.

$V_{Cr}(r, \phi)$ is the mean crystal potential that each of the three protons experiences and which contains all time-independent contributions due to neighbours acting on the reference ammonia molecule. Therefore the effective potential V_M that acts on the molecule in one specific setting (R_c, ϕ_c, β) is given by the sum of the contributions from each single atom

$$V_M(R_c, \phi_c, \beta) = \sum_{p=0}^{2} V_{Cr}(r_p, \phi_p). \tag{2}$$

The Boltzmann probability of finding a molecule with a given setting (R_c, ϕ_c, β) is

$$\rho(R_c, \phi_c, \beta) = Z^{-1} \exp[-V_M(R_c, \phi_c, \beta)/kT] \tag{3}$$

where Z is the partition function. The observed two-dimensional density distribution is proportional to the probability density function, which expresses the probability of finding one of the protons at a place (x, y). To calculate this function the contributions from all possible settings have to be summed up. As shown in [20] the two-dimensional density distribution $\rho(x, y)$ finally is derived as

$$\rho(x, y) = 3Z^{-1} \exp[-V_{Cr}^0(x, y)/kT] \int \exp[-(V_{Cr}^1 + V_{Cr}^2)/kT] \, d\gamma \tag{4}$$

with

$$V_{Cr}^1 = V_{Cr}(x + \sqrt{3}d_p \cos\gamma, y + \sqrt{3}d \sin\gamma) \tag{5}$$

$$V_{Cr}^2 = V_{Cr}(x + \sqrt{3}d_p \cos(\gamma + \pi/3), y + \sqrt{3}d \sin(\gamma + \pi/3)). \tag{6}$$

4.2. Potential refinement

We determine the potential parameters A, B, C and the distance d_p between the protons and the CM of the proton triangle by a least-squares analysis, by minimizing the residual

$$R = \sum_{x_i, y_i} [\rho_{\text{Boltzmann}}(x_i, y_i) - \rho_{\text{obs}}(x_i, y_i)]^2.$$

As input data we take the two-dimensional sections through the hydrogen/deuterium density shown in figure 2. In addition, we introduce a scaling factor and an additive constant c that accounts for the difference between the actual averaged scattering density and the averaged scattering density when only non-hydrogen atoms are considered. As shown earlier and more explicitly for the $Ni(NH_3)_6I_2$ data in [21], good agreement between the observed and calculated densities is achieved. The final parameters for all measured samples are summarized in table 2.

Table 2. Results of the potential refinement. A negative 'scale' transforms the negative scattering density of the protons into the number density.

	A (Å^2)	B (Å^4)	C (Å^4)	d_p (Å)	Scale	c	R^a	R_w^b
$Ni(ND_3)_6Br_2$	−468.9(2)	344.7(12)	1206.6(29)	0.9643(4)	2.597(3)	−0.002(1)	0.072	0.067
$Ni(NH_3)_6Br_2$	−288.2(1)	243.2(6)	868.8(19)	0.9654(4)	−1.474(1)	0.0112(7)	0.052	0.043
$Ni(NH_3)_6I_2$	−232.3(2)	166.0(1)	776.1(18)	0.9594(4)	−1.304(1)	0.043(1)	0.070	0.059
$Ni(NH_3)_6(NO_3)_2$	−56 1(1)	68.3(2)	282.8(6)	0.9183(4)	−0.2737(2)	0.0351(4)	0.045	0.047
$Ni(NH_3)_6(PF_6)_2$	−50.4(2)	23.6(8)	712.9(12)	0.9564(4)	−3.079(3)	0.0357(4)	0.079	0.065

[a] $R = \sum_{i=1}^{N_x} \sum_{j=1}^{N_y} |\rho_o(x_i, y_i) - \rho_c(x_i, y_i)| / \sum_{i=1}^{N_x} \sum_{j=1}^{N_y} |\rho_o(x_i, y_i)|$.

[b] $R_w = (\sum_{i=1}^{N_x} \sum_{j=1}^{N_y} w_{ij} [\rho_o(x_i, y_i) - \rho_c(x_i y_i)]^2 / \sum_{i=1}^{N_x} \sum_{j=1}^{N_y} w_{ij} \rho_o(x_i, y_i)^2)^{1/2}$.

All parameter sets found obey the relations $A < 0 < B < C$ so that the potential minima occur at $\phi_m = 45° \pm n \times 90°$ and the saddle points at $\phi_s = 0° \pm n \times 90°$. Figure 4 shows $V_{Cr}(x, y)$ calculated with the refined potential parameters given in table 2. From figure 4 it is easily seen that the deepest minima are found for $Ni(ND_3)_6Br_2$ and $Ni(NH_3)_6Br_2$. They are much weaker for $Ni(NH_3)_6I_2$; for $Ni(NH_3)_6(NO_3)_2$ they only show up as a slight modulation, while for $Ni(NH_3)_6(PF_6)_2$ they are not visible. Simultaneously the overall shape of the potential becomes increasingly more rotationally symmetric within this order.

To make a comparison between the different potentials easier, figure 5 shows one-dimensional cuts through the potentials of figure 4, where the potential minima define the zero level. From the difference in the location of the potential minima, shown in the cuts along the diagonal (x, x) and along the axis $(x, 0)$, the deviation from rotational symmetry is obvious. Again the height of the central maximum and the depth of the minima, compared to the height of the saddle points, are found to diminish in the sequence $Ni(ND_3)_6Br_2$, $Ni(NH_3)_6Br_2$, $Ni(NH_3)_6I_2$, $Ni(NH_3)_6(NO_3)_2$, $Ni(NH_3)_6(PF_6)_2$. In addition the radial distance of the minima r_m and saddle points r_s becomes smaller. This order reflects the increasing ionic radius r_{ionic} in the series Br, I, NO_3, PF_6 and, in the latter cases, tendencies towards a non-crystallographic eightfold symmetry, which will be discussed later. Figure 6 shows the dependence of the potential parameters r_m and r_s on r_{ionic}. Here we have chosen $r_{ionic} = 1.96, 2.20, 2.52, 2.98$ Å for Br [25], I [25], NO_3, PF_6, respectively. For NO_3 we choose $r_{ionic}(NO_3) = r_{NO} + r_{ionic}(O)$, where r_{NO} is taken from [18] and $r_{ionic}(O) = 1.32$ Å [25]. For the PF_6 group the effective ionic radius may be estimated from the crystal structure data [24]: the sum of the P–F distance (1.54 Å) and the fluorine ionic radius of 1.33 Å [25] amounts to 2.87 Å. We obtain a comparable value of 2.98 Å from the observation (Fourier densities [24]) that in the crystal structure two PF_6 groups are in contact.

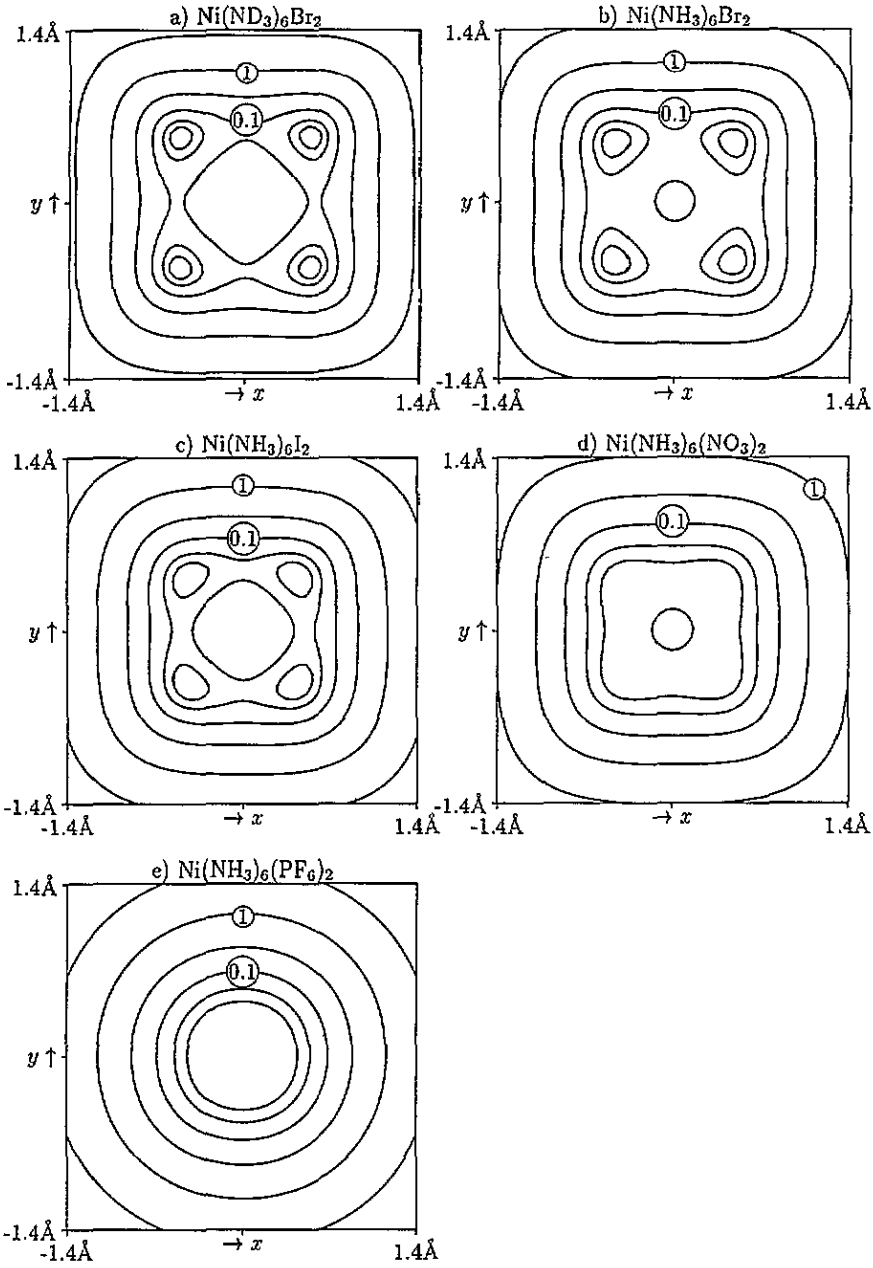

Figure 4. Mean crystal potential $V_{Cr}(x, y)$ normalized to the temperature of the measurement ($T = 295$ K) on a logarithmic scale: (*a*) $V_{Cr}[Ni(ND_3)_6Br_2]/T$; (*b*) $V_{Cr}[Ni(NH_3)_6Br_2]/T$; (*c*) $V_{Cr}[Ni(NH_3)_6I_2]/T$; (*d*) $V_{Cr}[Ni(NH_3)_6(NO_3)_2]/T$; (*e*) $V_{Cr}[Ni(NH_3)_6(PF_6)_2]/T$.

5. The effective molecular potential

To get information about the underlying dynamics of the molecule, which leads to the observed density distribution, the effective molecular potential V_M, as defined in (2), has to

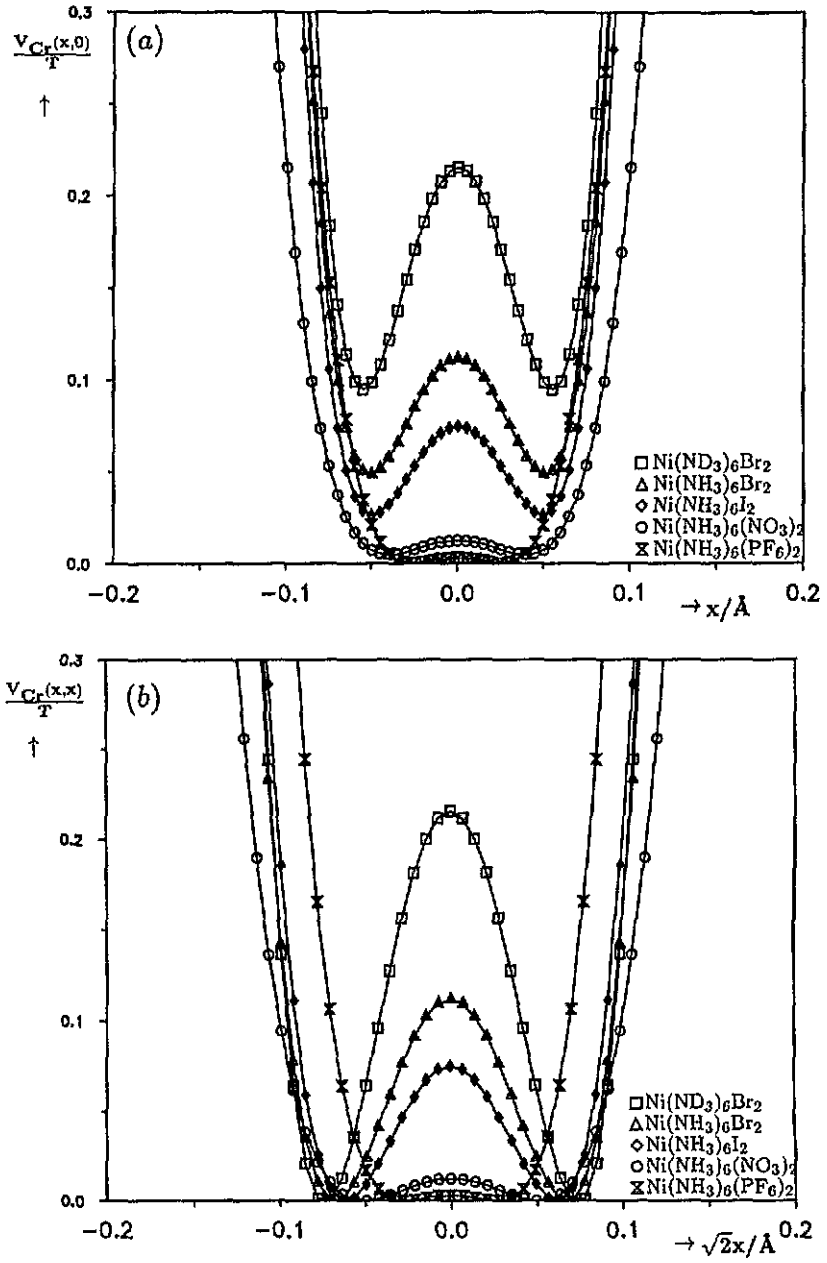

Figure 5. One-dimensional cuts through V_{Cr}: (*a*) $V_{Cr}(x, 0)/T$; (*b*) $V_{Cr}(x, x)/T$.

be considered. V_M can be reorganized as

$$V_M(R_c, \phi_c, \beta) = V_M^0 + V_M^R(R_c) + V_M^W(R_c, \phi_c, \beta) \tag{7}$$

with

$$V_M^0 = 3(\tfrac{1}{2}Ad_p^2 + \tfrac{1}{4}Cd_p^4) \tag{8}$$

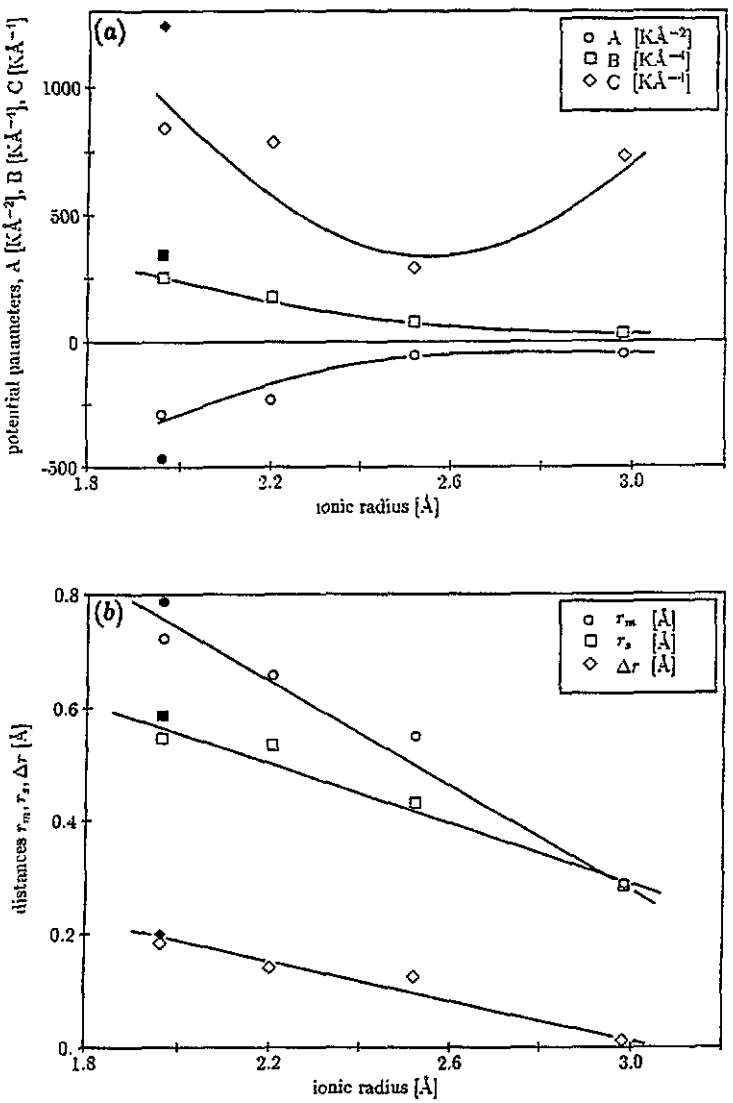

Figure 6. (*a*) Potential parameters and (*b*) distance of the potential minima and saddle points versus ionic radii of the nearest-neighbour complex anion. The interpolating curves are guides for the eye.

$$V_M^R(R_c) = 3[\tfrac{1}{2}(A + 2Cd_p^2)R_c^2 + \tfrac{1}{4}CR_c^4] \tag{9}$$

$$V_M^W(R_c, \phi_c, \beta) = 3[Bd_p^3 R_c \cos(4\phi_c + 3\beta) + \tfrac{1}{4}BR_c^4 \cos(4\phi_c)]. \tag{10}$$

V_M^0 is a constant term, which causes a zero shift in the potential and therefore is irrelevant for our further considerations. $V_M^R(R_c)$ depends only on the distance of the CM of the H_3/D_3 triangle to the fourfold axis and corresponds to an average over the angle-dependent potential terms. Even if the pseudoharmonic term $\frac{1}{2}Ar^2$ in the underlying crystal potential V_{Cr} vanishes, the resulting molecular potential has a true harmonic contribution ($A_M = A + 2Cd_p^2 > 0$). The last term V_M^W expresses the coupling of the CM position and

the orientation of the triangle. Consequently it depends on R_c, ϕ_c and β and is dominated by the parameter B, which gives the strength of the coupling. With given $R_c = 0$ the *effective molecular potential* ($V_M(0, \phi_c, \beta) = V_M^0$) *is independent of both* ϕ_c *and* β. This is a direct consequence of the fourfold symmetry of V_{Cr} combined with the threefold molecular symmetry. With increasing R_c the three- and fourfold periodicities of V_M show up and the absolute potential minima occur under a defined value $R_c^m \neq 0$ and corresponding angles (ϕ_c^m, β^m). Figure 7 shows a cut through $V_M(R_c, \phi_c, \beta)$ at $R_c = R_c^m$ where the absolute potential minimum is found. The overall shape is identical for the five refined parameter sets. But the values for R_c^m decrease from 0.16 to 0.02 Å and the magnitude of the potential wells decreases from 293 to 2 K from $Ni(ND_3)_6Br_2$ to $Ni(NH_3)_6(PF_6)_2$.

	R_c^m	ΔV_M
$Ni(ND_3)_6Br_2$	0.16 Å	293 K
$Ni(NH_3)_6Br_2$	0.15 Å	198 K
$Ni(NH_3)_6I_2$	0.12 Å	102 K
$Ni(NH_3)_6(NO_3)_2$	0.12 Å	38 K
$Ni(NH_3)_6(PF_6)_2$	0.02 Å	2 K

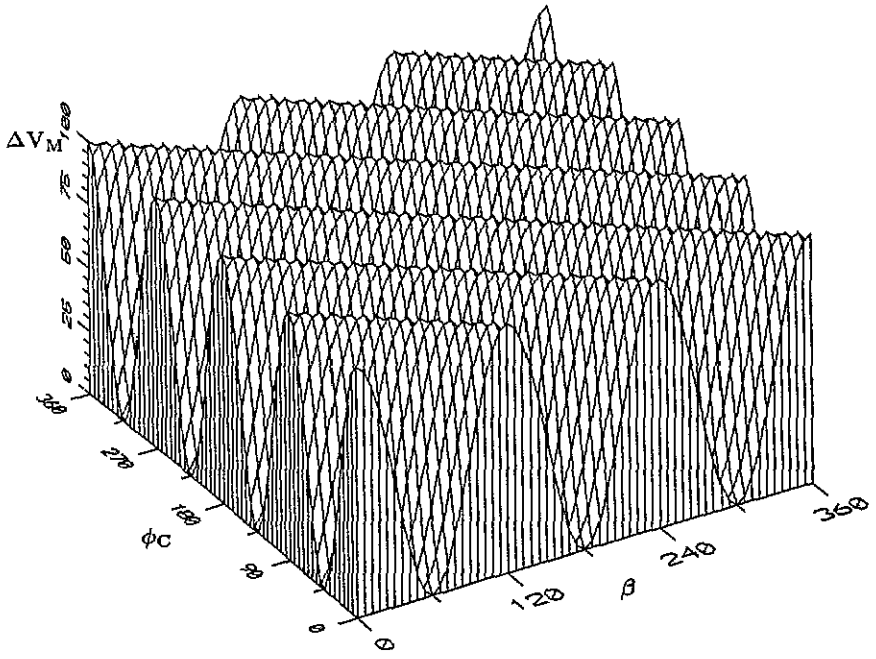

Figure 7. Effective molecular potential $V_M(R_c, \phi_c, \beta)$ for fixed CM radius $R_c = R_c^m$, where the absolute potential minimum is reached. A jump across a maximum corresponds to a rotation of the molecule by 120° about an axis passing through its CM.

For all potentials obtained the absolute potential minima are found under $\phi_c = 45° + n \times 90°$ and $\beta = 0° + n \times 120°$. For small values R_c the term proportional to $\cos(4\phi_c + 3\beta)$ in (10) dominates. As shown in figure 7 this leads to linear elongated potential minima valleys with a negligible modulation $\sim R_c^4 \cos(4\phi_c)$. Because $V_M(R_c, \phi_c, \beta)$ is

periodic with ϕ_c and β, figure 7 actually shows the surface of a torus and therefore all the valleys are topologically equivalent. Thus there exists only one single path through the valleys, which is defined by

$$\phi_c = (2n + 1) \times 45° - \tfrac{3}{4}\beta. \tag{11}$$

Moving through this minimum valley, both ϕ_c and β run through the whole angular region from 0° to 360° but linearly coupled with $4\phi_c/3\beta = \text{const}$ according to (11). Assuming a motion of the molecule strictly following the minimum valleys of the effective molecular potential V_M allows one to calculate the orbit of the protons. For $R_c^m \neq 0$ the coupling (11) between ϕ_c and β results in hypocycloids as orbits. Some of them are shown in figure 8. Clearly they show the desired fourfold symmetry, while each of the three protons moves on the same orbit with a delay of 120° in β. In addition for small R_c^m, as found in $Ni(NH_3)_6(PF_6)_2$, the orbit is nearly rotationally symmetric, which in turn is in agreement with the nearly rotational density distribution found in this compound.

6. Discussion and conclusions

The model we suggest is a modification and extension of the Bates–Stevens (BS) model [10] used earlier to interpret relaxation times in electron paramagnetic resonance (EPR) experiments: the BS model allows every X_3 triangle to rotate by a discrete angle about the fourfold averaged crystal axes with the X_3 plane perpendicular to these axes. We retain the latter orientation of the hydrogen/deuteron plane with respect to the crystal axes. The crystal potential model (equations (1)–(10)) uses three instead of one (BS) degrees of freedom, and it applies Boltzmann statistics as an essential ingredient. The possibility of a tumbling motion, which we showed to be present in the actual observation to a minor degree [19–21, 24], is not taken into account in either the BS or our rotation–translation model. Tumbling motions have been considered, however, recently by Press *et al* [26].

The fourth-order potential parameters B and C are correlated in a non-linear way with the effective ionic radii r_{ionic} (figure 6(*a*)). There is, however, a fairly good linear correlation between the parameters B, C and the minimum and the saddle point distances r_m and r_s, respectively, as shown in figure 6(*b*). From this figure we can actually conclude again that $Ni(NH_3)_6(PF_6)_2$ has an isotropic circular potential. This observation is in good agreement with the tunnel splitting observed in this compound, 540 μeV, which comes close to the level distance $\Delta E = E_{l=1} - E_{l=0} = B = 690$ μeV [27, 28] between the first excited and the ground state of the free rotator. The reason for this correlation becomes evident from figure 9, which illustrates the extension of the electron clouds of the Y (simple or complex) anions in the plane $z = 1/4$. The centre circle in figure 9 is the orbit of an X_3 group rotating about [001]. Actually the highest proton density is found at the levels $z/a = 0.24$, 0.23, 0.23, 0.21 for Y=Br, NO_3, PF_6 respectively; only for Y=PF_6 are the X_3 and the anion planes slightly separated. The variation of the anisotropy of V_{Cr} in the given series of compounds is (figures 4, 5 and 9) the result of the confinement of the X_3 group by the anions: a geometrically narrow restriction, as for Y=Br, I, showing in addition clearly that fourfold symmetry favours an anisotropic distribution. In the case of Y=NO_3, PF_6, there is, first, a larger distance between the H/D circle shown in figure 9 and the ions, and so the potential is weaker. More important is however, secondly, that in these compounds the ionic density distribution comes fairly close to a local, non-crystallographic eightfold symmetry, which is a natural explanation for the weak fourfold Fourier component of the crystal potential.

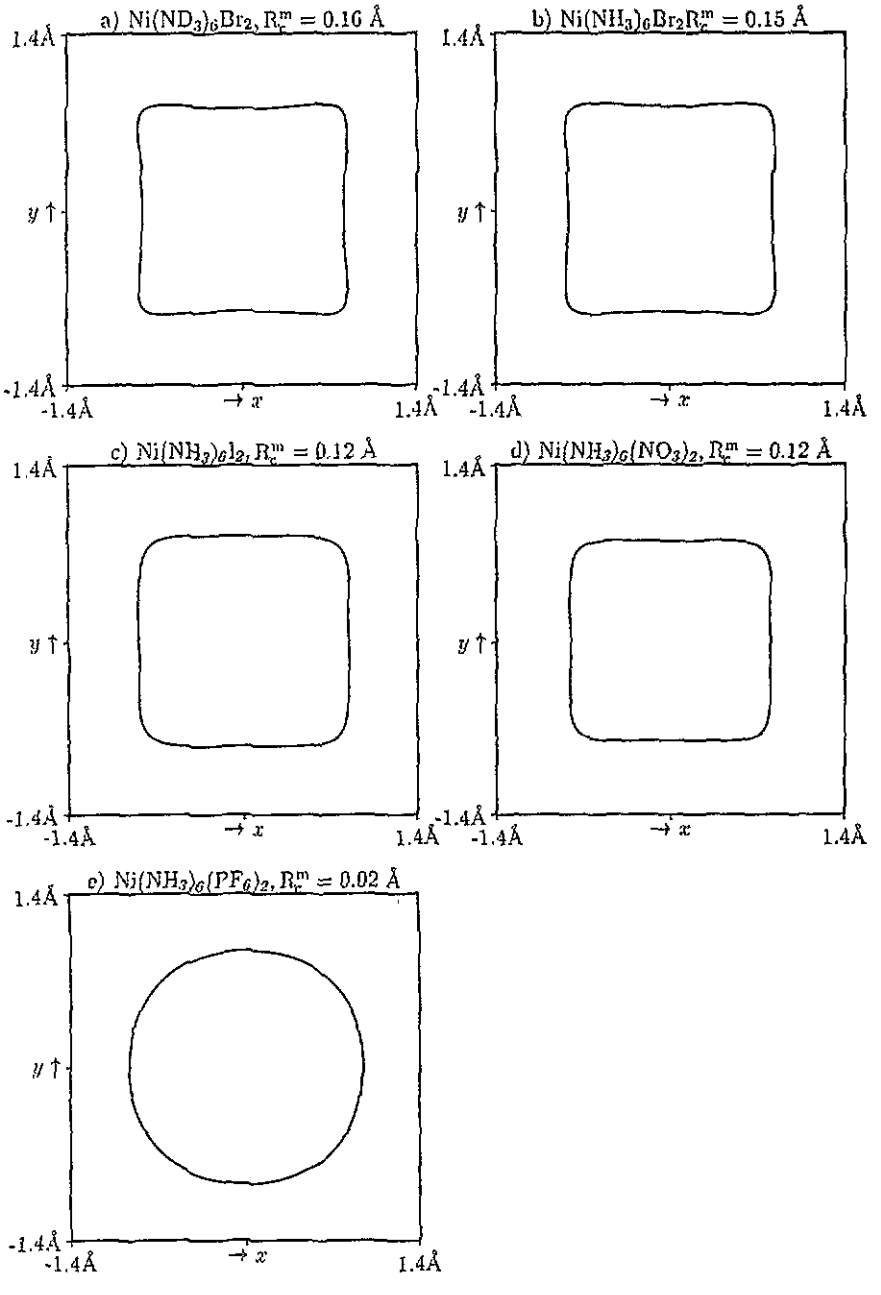

Figure 8. *The hypocycloids, i.e. orbits of the protons corresponding to a motion at constant* CM radius, strictly following the potential minimum valleys.

The actual motion of the NH_3/ND_3 molecules in the anisotropic potential may be easily derived from the effective molecular potential $V_M(R_c, \phi_c, \beta)$. V_M has, within the series Y = Br..., PF_6, an absolute minimum at a certain CM distance, say R_c^m. As a function of ϕ_s and β, $V_M(R_c^m, \phi_s, \beta)$ has, for all the compounds studied, the same general feature (figure 7), namely a sequence of waves with the coordinate of the valley given by

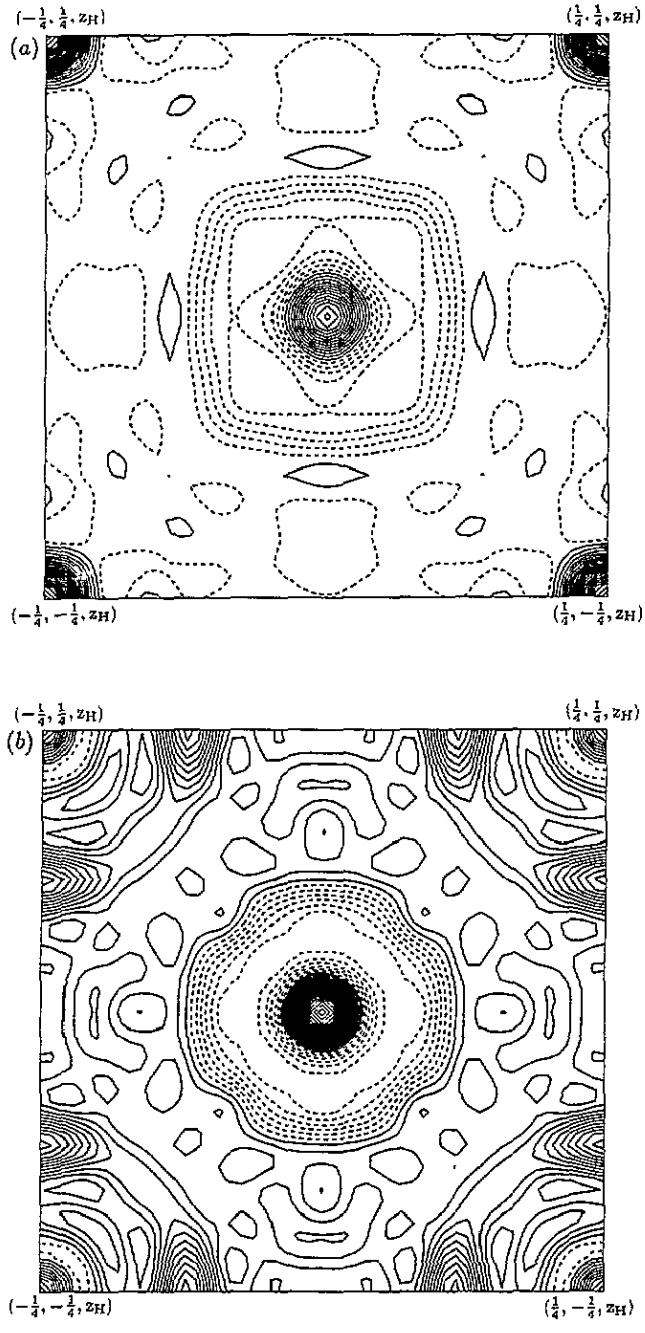

Figure 9. (*a*) The density of $Ni(NH_3)_6I_2$ at $z_H = 0.23a$, i.e. the level of the hydrogen plane. (*b*) The same for $Ni(NH_3)_6(PF_6)_2$ ($z_H = 0.21a$). In the latter case the phosphorus atoms occupy the corners, and the fluorines lie on the edges of the square: the pseudo-eightfold symmetry is clearly visible. The heavy atom in the centre of (*a*) and (*b*) having positive density is nitrogen located at $z_N = 0.20a$ (*a*) and $z_N = 0.18a$ (*b*): these atoms are visible due to the thermal motion. Hydrogen scattering densities (negative) are shown as dashed lines. The heavy ring outside the H density in (*b*) as well as some minor local fluctuations in (*a*) are due to series termination effects.

$$\phi_s = n\pi/2 - \tfrac{3}{4}\beta. \tag{12}$$

These valleys are, for $R_c = R_c^m$, completely flat. A molecule may move 'along the valley' without experiencing a hindrance potential. For $R_c > R_c^m$ the wavy nature of V_M becomes more complicated: the bottom level of the valleys as well as the top of the waves become modulated. We show in figure 8 the orbits of the proton for Y=Br, I, NO_3, PF_6. In all cases the ϕ_s to β coupling (12) is obeyed, and the differences in the shape of the orbits are exclusively due to the numerical values of R_c^m.

We return to the question about the origin of the hindrance potential in the nickel hexammine compounds addressed earlier several times [8, 10]. From figure 9 it is evident that the ammine groups are strongly confined by the Y anions. This confinement does not eliminate the electrostatic interaction considered by BS. From the analysis presented so far, however, it is clear that the hydrogen bonds established in a dynamic way between three protons and four complex anions are an essential driving force for the anisotropic motion. The rotation–translation coupling we observe is the result of a subtle interplay between geometrical confinement and the frustration of these hydrogen bonds, for which figure 9 is an illustration: the hypocycloidal motion is generated by one proton/deuteron X_1 being in or close to the energy minimum of its hydrogen interaction potential with one anion Y^a. By thermal agitation X^1 leaves its bond, and X^2 or X^3 establish a bond with Y^b. In the idealized case this motion would occur only along the valleys of V_m. There would be no need to overcome an activation barrier, and therefore the motion would be purely diffusive. We have found, indeed, from molecular-dynamics simulations [24] that, at sufficiently low temperatures, the orbits shown in figure 8 are reproduced also. At higher temperatures, chaotic orbits occur, and increasing the temperature in the simulations still further, free rotations show up even for the most anisotropic crystal potentials as e.g. in $Ni(NH_3)_6Br_2$.

Acknowledgments

This investigation was supported by the BMFT as project 02-PR2-TUE and by the DFG as project PR44/7-1.

References

[1] Palma-Vittorelli M B, Palma M V, Drewes G W J and Koerts W 1960 *Physica* **26** 922–30
[2] Asch L, Shenoy G K, Friedt J M, Adloff J P and Kleinberger R 1975 *J. Chem. Phys.* **62** 2335–42
[3] Klaaijsen F W, Suga H and Dokoupil Z 1971 *Physica* **51** 630–3
[4] Andresen A F, Fjellvåg H, Janik J A, Mayer J, Sciesinski J, Janik J M, Migdal-Mikuli A, Mikuli E, Rachwalska M and Stanek T 1986 *Physica* **138B** 295–304
[5] Eckert J and Press W 1980 *J. Chem. Phys.* **73** 451–60
[6] Bates A R, Ferris L T H and Jenkins T E 1979 *J. Phys. C: Solid State Phys.* **12** 2945–55
[7] Janik J M, Janik J A, Migdal-Mikuli A, Mikuli E and Otnes K 1991 *Physica* B **168** 45–52
[8] Blank H and Kearley G J 1988 Private communication
[9] Kearley G J and Blank H 1988 *Can. J. Chem.* **66** 692–7
[10] Bates A R and Stevens K W H 1969 *J. Phys. C: Solid State Phys.* **2** 1573–85
[11] Bates A R, Crick J L A and Davies R O 1976 *J. Phys. C: Solid State Phys.* **9** 3013–36
[12] Elgsaeter A and Svare I 1970 *J. Phys. Chem. Solids* **31** 1405–8
[13] Jenkins T E and Bates A R 1981 *J. Phys. C: Solid State Phys.* **14** 817–27
[14] Hodorowicz S and Ciechanowicz-Rutkowska M 1978 *Acta Phys. Polon.* A **53** 29–32
[15] Janik J A, Janik J M, Migdal-Mikuli A, Mikali E and Otnes K 1988 *Acta Phys. Polon.* A **74** 423–31
[16] Janik J A, Janik J M, Migdal-Mikuli A, Mikuli E and Otnes K 1986 *Acta Phys. Polon.* A **70** 603–8

[17] Janik J M and Janik J A 1975 *Acta Phys. Polon.* A **48** 311–13
[18] Hoser A, Joswig W, Prandl W and Vogt K 1985 *Mol. Phys.* **56** 853–69
[19] Hoser A, Prandl W, Schiebel P and Heger G 1990 *Z. Phys.* B **81** 259–63
[20] Schiebel P, Hoser A, Prandl W and Heger G 1990 *Z. Phys.* B **81** 253–8
[21] Schiebel P, Hoser A, Prandl W, Heger G and Schweiss P 1993 *J. Physique* **3** 987–1006
[22] Gmelin 1968 *Gmelins Handbuch der Anorganischen Chemie Nickel* Part C 1, No 57, 8th edn (Weinheim: Verlag Chemie)
[23] Sheldrick G M 1976 *SHELX-76 A Computer Program for Crystal Structure Determination* University of Cambridge
[24] Schiebel P 1993 *Dissertation* Universität Tübingen
[25] Weast R C 1985 *Handbook of Chemistry and Physics* 66th edn (Oxford: CRC)
[26] Press W, Nöldeke C, Schröder-Heber A, Prandl W and Schiebel P 1993 *Acta Crystallogr.* A **49** 729–35
[27] Kearley G unpublished results, quoted in [28]
[28] Prager M and Heidemann A 1987 *ILL Internal Report* 87PR1ST